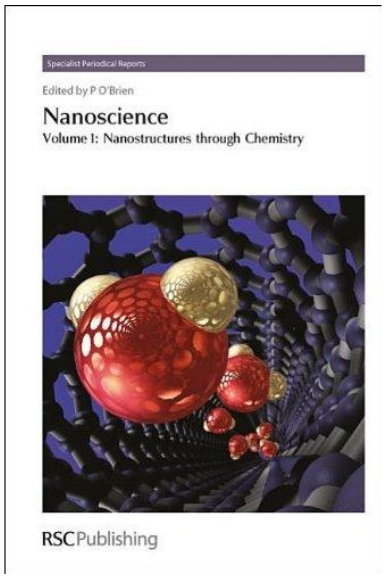

D. Ortega and Q. A. Pankhurst, *Magnetic hyperthermia*, in *Nanoscience: Volume 1: Nanostructures through Chemistry*, P. O'Brien, Editor. 2013, Royal Society of Chemistry: Cambridge. p. 60-88

DOI: 10.1039/9781849734844-00060

3 Magnetic hyperthermia

Daniel Ortega*[a,b] and Quentin A. Pankhurst[b,c]

DOI: 10.1039/9781849734844-00060

Magnetic particle hyperthermia is potentially the most significant and technically disruptive of the currently known biomedical applications of magnetic nanoparticles. Recent developments indicate that this highly specific and targetable method of localised remote heating of bodily tissue could revolutionise clinical practice in the treatment of cancer, either as an adjunct to radiotherapy and chemotherapy, or as a stand-alone intervention. In this chapter we review some of the recent technical advances that have been made in magnetic hyperthermia, and comment on its translational prospects with regard to improving the treatments of cancer patients.

1 Introduction

Although there has been a decline in cancer death rates since the early 1990s,[1] the disease is still the most common cause of death in the UK and the second one in the US, killing 157,275 and 569,490 people in both countries in 2010, as reported by the Cancer Research UK and the National Cancer Institute.[2, 3] There is therefore a pressing need for either improving the existing therapies or developing new ones to improve survival rates.

Existing therapies face fundamental challenges that stem from the biology of the disease. Cancers are characterized by their unregulated growth and spread of cells to other parts of the body through the bloodstream or the lymphatic system.[4] Once deposits of malignant cells start to form, the process of forming new blood vessels (angiogenesis) takes place leading to a chaotic vascularisation, unlike normal tissue. This feature is shown in Fig. 1, where differences in vascular branching pattern and density between both types of tissues can be clearly appreciated. As a consequence of the defective blood perfusion, tumours and the surrounding tissues present a low pH and low oxygen pressure (hypoxia). In these conditions, radiotherapy is less effective and cytotoxic drugs reach the affected regions in a much lower concentration than the aimed therapeutic dose.

Aimed to circumvent, or at least alleviate, these problems, *clinical hyperthermia* – the therapeutic approach whereby elevated temperatures damage and/or kill malignant cancer cells within the body – is an attractive approach, given the relatively non-specific nature of heat treatment. It has already been used with some success as a adjunct to radiotherapy and chemotherapy, with some synergistic effects having been observed.[5, 6] That said, the design parameters of hyperthermia treatments inevitably do still rely in part on the cancer biology. In particular these include the *therapeutic window*, which is the temperature range within which pathogens are more susceptible to heat than healthy tissue (typically between 40 and 44 ºC) – which depends both on the affected part of the body and the mode of heating; and the *thermal dose-response* of the tissue, which is largely determined by local environmental factors in the vicinity of the tumour.

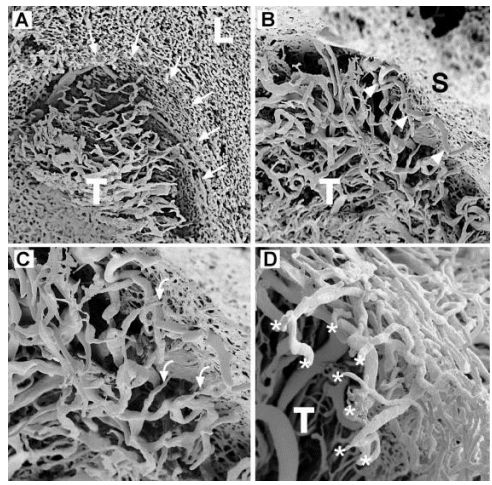

Fig. 1 (a) Scanning electron microscopy image showing the boundary between normal liver (L) and tumour (T) formed by compressed sinusoids (arrows). Tumour vessel density is less than that of surrounding normal liver (original magnification×70). (b) Closer view of tumour and liver boundary formed by compressed sinusoids (S). Tumour (T) vessels show complex branching and spiral configuration and arise from the tumour margins (arrow heads) (original magnification×120). (c) Direct branches connecting sinusoids to tumour vessels (arrows) (original magnifications×210). (d) Sinusoidal branches extending to and ending abruptly (*) at the tumour-liver interface (original magnification×140). Reprinted from Ref.[7], copyright (2003), with permission from Elsevier.

In a first approximation, hyperthermia treatments can be classified into three broad categories: whole-body hyperthermia, regional hyperthermia and local hyperthermia.[8] The first one is often used in metastatic cancer cases, whereas the latter two are more appropriate for localised tumours. The current technology on whole-body hyperthermia has been recently reviewed.[9] Local hyperthermia can be in turn further classified into other subcategories, namely, external, interstitial and endocavity hyperthermia. In addition, heat generation methods vary depending on the target region and include capacitive or inductive coupling of radiofrequency fields, microwave radiation, ultrasound, perfusion therapy, interstitial laser photocoagulation and heat administered by external contact.[10]

Although there are evidences supporting the knowledge of hyperthermia as a common practice to treat certain ailments since 300 BC,[11] it has not been until the last two decades that a substantial improvement in both methodology and integration with adjunct treatments has been achieved, along with more creditable results. The joint efforts of experts in chemistry, engineering, medicine and physics have played an important role, as exemplified by the numerous reviews published on the matter.[12-20] There is a twofold reason for these emergent collaboration networks. First, the incorporation of nanotechnology has opened a new way of re-interpreting the technique, in terms of a better localization of tumours and access to regions difficult to reach inside the human body are now possible. Second, and distinct from the development of new materials and technologies, the growing interest in hyperthermia research has been encouraged by the promising results obtained in clinical trials dealing with different kinds of cancer at different stages,[17, 21] showing enhanced survival rates.

The search for more versatile and efficient hyperthermia techniques relies upon several key facts:

1. Early stage cancer entities are usually localised, but in the case of deep tissues, access is awkward and a therapeutic heat dose is difficult to be conveniently delivered. The activation issues related to the infrared radiation used in whole-body and local hyperthermia techniques exemplify this limitation.
2. A major challenge for any thermotherapy is the preservation of healthy tissue while ensuring a complete removal of the malignant one.
3. Due to the changing physiological parameters during a hyperthermia session (blood perfusion, oxygen pressure, etc.), there are serious restrictions in order to sustain a homogeneous temperature distribution in the target tissue region.
4. Although hyperthermia is a well known radio- and chemo-sensitiser,[17] and its adverse effects are in principle milder than those of cytotoxic drugs and radiotherapy, the latter cannot be completely replaced with the existing hyperthermia techniques. As systemic treatments place the entire physiology under severe strain, the establishment of a hyperthermia modality aimed for thermal killing – referred to as *thermoablation* – would be preferred in some cases. However, this would require higher temperatures (over 50 ºC) that could increase the risk of severe or persistent side effects in proportion to the size of the target region.
5. Heat shock proteins (HSP), encoded by heat shock genes in response to thermal stress are regarded as a complicating factor in hyperthermia, as these are implied in the development of transient thermotolerance and permanent heat resistance of cells.[22] This would hamper the efficacy of the current thermotherapies.

Magnetic particle hyperthermia (also called magnetic field hyperthermia or sometimes just magnetic hyperthermia) was introduced and tested by Gilchrist in 1957 as a means to heat lymph nodes in dogs.[23] Subsequent work by the same group showed progress towards a variant for humans.[24, 25] Magnetic nanoparticles under the action of an externally applied alternating current (AC) field can generate a certain amount of heat proportional to the frequency of that field.[16] Because of the requisite small size of the particles – typically of the order of hundreds of nanometres – the use of this effect is set to revolutionize the existing hyperthermia procedures, as it offers the possibility of heating the targeted tumoural tissue while preserving the healthy tissue, as attested by successful results in clinical trials.[26] In addition, magnetic particle hyperthermia offers the possibility of frequent repeated treatment. In short, magnetic nanoparticles with enhanced heating capabilities, along with the techniques for probing them, have profoundly transformed the way in that hyperthermia-based therapies are structured, leading to an exciting new concept in cancer treatment, among other diseases.

In summary, magnetic particle hyperthermia aims to address the aforementioned five issues, and others, by virtue of some unique characteristics:

- It is a truly local therapy; just the region containing magnetic particles will be treated.
- Given the small area of action, thermoablation at moderately high temperatures under strictly controlled conditions becomes feasible for treating some types of cancer, since the associated side-effects should be much reduced.
- Recent advances in chemistry have allowed bioconjugated magnetic particles to be specifically targeted to cancer cells, hence sparing healthy tissue while killing the malignant cells becomes a possibility.
- Relatively recent studies show that it would be possible to take advantage of the HSP expression activated by hyperthermia through the application of an AC

field. [27] As well as HSP expression, controlled hyperthermia also increases the levels of MHC (major histocompatibility complexes) class I peptides at the surface of tumour cells, whose function is to expose selected protein fragments of cells to cytotoxic T lymphocytes. This causes an immunoresponse, where healthy cells are ignored and cancer cells are attacked.

2 Physical principles of magnetic hyperthermia

There are three length scales levels involved in the heat transfer mechanisms involved in AC hyperthermia, namely: (i) nano-scale, defined by the size of the magnetic particles (5±100 nm); (ii) micro-scale, characterised by the cells size (5±20 μm); and (iii) macro-scale, determined by the size of the target tissue (typically up to 20 mm).[28] On the other hand, depending on the choice of magnetic material – but not necessarily on the aforementioned length scales - heat can be generated by virtue of the following mechanisms:[29]

- Seeds/beads: resistance heating due to *eddy currents*
- Multi-domain particles: magnetic heating due to *hysteresis loss*
- Nanoparticles: magnetic heating due to *Néel and Brownian relaxation* processes

These will be covered in the following sections, paying attention to the underlying physics and the implications on magnetic particle hyperthermia.

2.1 Eddy currents

Following the Faraday-Lenz law of electromagnetic induction, when an AC field penetrates a conducting sample, the associated time-varying magnetic flux will induce the evolution of eddy currents opposing to the applied field. This results in a field attenuation, which will depend on the field frequency, the electrical conductivity of the material and its permeability. Eddy currents are not exclusive of magnetic materials and also occur in tissues; nevertheless, the low specific electrical conductivity of the latter (0.6 $(\Omega m)^{-1}$, about eight orders of magnitude smaller than in metals)[30] produces a heating effect very distant from a practical therapeutic dose. The contribution from eddy currents in small particles is assumed to be rather small since the heating power decreases with decreasing particle size, as previously demonstrated.[31]

2.2 AC hysteresis losses

The magnetic structure of ferromagnetic materials is spontaneously split into *domains*, which are regions grouping magnetic moments with the same orientation. When the material is subjected to a cycle of positive and negative magnetic fields, the magnetisation shows a non-linear behaviour, described by a singular representation: the *hysteresis loop* (Fig. 2). Its three main parameters are:

- The *saturation magnetisation* (M_s) represents the limit value to which the curve tends within the high field region, and is reached when all the magnetic moments in the material are aligned with the external field.
- The *remanence* or *remanent magnetisation* (M_r), which is the retained magnetisation at zero field from the saturation state.
- The *coercivity* or *coercive field* (H_c) represents the field needed in order to completely demagnetise the sample.

In the case of a time-varying field, the area under this loop is related to the amount of heat generated per cycle (P_{FM}):[16]

$$P_{FM} = \mu_0 f \oint H dM \quad (1)$$

where f is the frequency of the applied field, H the field strength and M the magnetisation. For applications in medicine, frequencies in the range f = 0.05 - 1.2 MHz, and field strengths in the range H = 0 - 5 kA m^{-1}, are commonly used. During a hysteresis loop, there are two processes contributing to hysteresis losses; the first is the displacement of domain walls being pinned and released at inhomogeneities in the studied material, while the second is the rotation process of magnetic moments inside domains. The energy associated to the domain formation process increases with decreasing length scales, in such a way that if the size of a ferromagnetic-like material is reduced below a critical value, domain formation is no longer energetically favourable. Under these conditions, the magnetic structure of the whole material becomes a *single domain*. In the case of single domain particles, hysteresis losses are higher than any of the other losses presented in subsequent sections.[32]

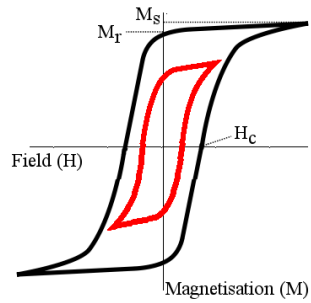

Fig. 2 Saturation hysteresis loop (black line) and minor loop (red line), with indication of the most representative parameters: saturation magnetisation (M_s), remanent magnetisation (M_r) and coercive field (H_c).

Contrary to the assumptions made in some simplified calculations, interparticle interactions have a marked effect in hysteresis losses.[33] This is in agreement with the interparticle distance dependence experimentally found in the heat generation capabilities of dextran-coated iron oxide nanoparticles.[34] For larger particles the energy loss per cycle is reduced due to the reduction of both H_c and M_r, while for smaller particles the energy loss is enhanced due to an enhancement of the anisotropy energy barriers separating the different orientation states, causing the blockage of the magnetisation in the case of superparamagnetic nanoparticles (see Section 2.3).

2.3 Relaxational losses

The set of individual magnetic moments inside a magnetic particle is usually represented by a single *super-spin* that accounts for the total magnetisation per particle. For particle sizes below a certain threshold value of typically tens of nanometres, thermal fluctuations may overcome the magnetic energy, causing a rapid flipping of the magnetisation away from its equilibrium state. This thermally activated process is called *superparamagnetism*.

The rotation of a system of magnetic nanoparticles suspended in a liquid carrier is

mainly governed by two relaxation mechanisms. The first involves a change in the orientation of all the spins in the particles and hence the magnetisation direction, but not necessarily a physical rotation of every particle; it is known as Néel relaxation. There is a characteristic time for the fluctuations of the magnetisation in a nanoparticle to occur, the *relaxation time* τ_N, and its temperature dependence was proposed by Louis Néel:[35]

$$\tau = \tau_0 \exp\left(E_B / k_B T\right) \tag{2}$$

where k_B is the Boltzmann constant and E_B the anisotropy energy barrier, being the latter proportional to the anisotropy constant of the material and the particle volume. The pre-exponential factor τ_0 is called *attempt time*, and it is assumed to be constant with a value within the range 10^{-9} – 10^{-13} seconds.

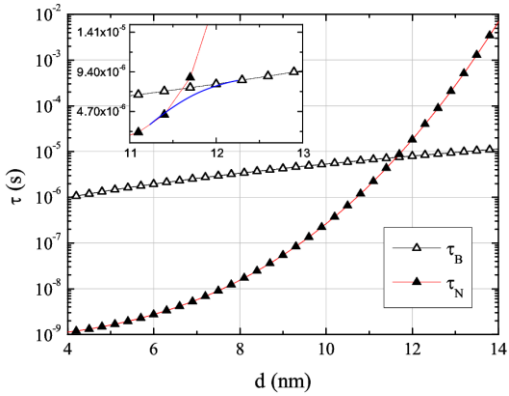

Fig. 3 Calculated Néel and Brown relaxation times over a range of particle sizes for a water-based magnetite colloid. Inset: geometric mean of τ_B and τ_N (blue line).

In the case of the second mechanism – the so-called Brown relaxation – particles can physically rotate to an extent dependant on the hydrodynamic parameters of both the particles and the medium, and at a characteristic time: [36]

$$\tau_B = 3V_h \eta / k_B T \tag{3}$$

where V_h denotes the hydrodynamic volume (obtained from the hydrodynamic diameter measured through dynamic light scattering, for example) and η the viscosity of the liquid carrier. Néel relaxation dominates over a short range of particle sizes as the fastest process and above a certain critical size, Brown relaxation mechanism takes over (Fig. 3). In the surroundings of that critical size, where both processes are equally probable, the net relaxation time τ is given by their geometric mean.[37]

The characteristic measurement time (τ_m) associated to a particular technique will determine whether or not the superparamagnetic behaviour of a sample will be observed during an experiment. In the case of AC magnetometry $\tau_m = 10^2$-10^4 s for low frequency experiments and $\tau_m = 10^{-1}$-10^{-5} s for classical experiments.[38] For a given system of nanoparticles, a superparamagnetic behaviour will be observed if $\tau_m < \tau$ and a ferromagnetic-like one if $\tau_m > \tau$.

It should be noted that the Néel-Brown relaxation model, although widely

employed throughout the literature for predicting and interpreting different parameters of interest in colloids for magnetic hyperthermia such as optimum particle size, frequency or field amplitude, has been criticised due to the disagreements found in both qualitative and quantitative analyses.[39-41] Some of these will be commented on in Sections 2.4.1 and 2.4.2.

2.4 Some parameters of interest in magnetic hyperthermia

2.4.1 Specific absorption rate / Intrinsic loss parameter

The amount of energy absorbed during exposure to an electromagnetic radiation is commonly estimated through the whole-body *specific absorption rate* (SAR):[42]

$$SAR = (\Delta T \cdot c) \cdot t^{-1} \tag{4}$$

where ΔT is the temperature increment, c the specific heat of the material being tested and t is the time of the sampling period. The equivalent term *specific loss power* (SLP) is also commonly found in the literature.

Although use of the SAR parameter has become widespread in the hyperthermia community to evaluate the heating capabilities of magnetic particles and to establish exposure limits, the outcomes from different experiments cannot be easily compared. Consequently, a new parameter has been proposed as a first approximation to allow a more direct comparison between results from measurements carried out in different laboratories under different field strengths and frequencies.[43] The so-called *intrinsic loss parameter* (ILP) is defined as:

$$ILP = \frac{P}{\rho H^2 f} = \frac{SAR}{H^2 f} \tag{5}$$

where P is the volumetric power dissipation $P = \mu_0 \pi \chi''(f) f H^2$, with $\chi''(f)$ the imaginary part of the magnetic susceptibility.[44]

Strictly speaking the ILP parameter is a low-field approximation to a more complex relationship, and is best used subject to the following conditions: (i) field frequencies of up to several MHz; (ii) polycrystalline samples with a polydispersity index (related to the size distribution width) of more than 0.1; (iii) applied field magnitudes well below the saturation field of the nanoparticles; and (iv) experimental conditions wherein environmental thermodynamic losses do not overwhelm the power input from the hyperthermic field. Nevertheless, even with these provisos, the ILP parameter is a useful comparator in any discussion of particle performance. For example, Fig. 4 shows the ILP values for a series of commercially available magnetic colloids as a function of particle diameter. Note that unlike the hydrodynamic diameter, size values in Fig. 4 are referred to the magnetic core without taking into account the surface coating. As a general trend, larger magnetic core particle sizes are associated with higher ILP values.

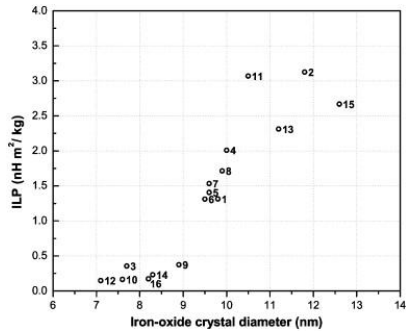

Fig. 4 ILP versus particle diameter. The mean diameter of a lognormal particle distribution for each sample was calculated by fitting a Langevin function to superparamagnetic hysteresis curve measured at 300 K. Within the given range of diameters, larger core particle sizes result in higher heating properties, particularly noticeable for Micromod's BNF series (3, 10, 12 and 16) that have relatively smaller particle diameters than the better heaters. [A full legend for this graph can be found in Ref. [43]]. Reprinted from Ref. [43], copyright (2009), with permission from Elsevier.

2.4.2 Safety limits and patient tolerance

It was previously noted that, for the most part, developers of magnetic hyperthermia applications for human therapies employ systems that deliver frequencies in the range f = 0.05 - 1.2 MHz, and field strengths in the range H = 0 - 5 kA m^{-1}. The origins of these essentially self-imposed limits are the subject of some debate, as is the question of whether there should be a unilaterally-imposed safety limit for the use of radio frequency fields for magnetic hyperthermia. The key issue here is whether non-specific heating or other damaging effect may occur in the human body when subjected to the alternating field. The most likely source of such damage is eddy current heating, an electrical effect where currents are induced in a conductor (in this case the water in the human body) due to a changing magnetic field.

In 1984, Atkinson[45] considered eddy current effects, and the implications these might have on usable frequencies and field strengths for hyperthermia. He estimated that the rate of heat production per unit tissue volume for a cylindrical body (he was envisaging a human arm or torso) placed inside a long solenoid delivering a uniform magnetic field H over the entire volume is:

$$P_{eddy} = \sigma_t (\pi \mu_o)^2 H^2 f^2 r^2 \quad (6)$$

where σ_t is the electrical conductivity of the tissue, and r the radius of the cylinder. One point to notice immediately from Eq. 6 is that the heating effect of a given field and frequency on a human arm ($r \approx 5$ cm) will be 16x less than on a torso ($r \approx 20$ cm). Atkinson also performed some clinical tolerance tests using a single-turn induction coil placed around the thorax of healthy volunteers, and found that "field intensities up to 35.8 A·turns/m at a frequency of 13.56 MHz can be thermally tolerated for extended periods of time".

It is perhaps remarkable that in the ensuing decades, this clinical tolerance test does not yet appear to have been repeated. Instead, the results reported by Atkinson have become enshrined in an often-quoted 'safety limit' for hyperthermia field frequency and amplitude, the 'Brezovich criterion'[46] that the product $C = H \cdot f$ should not exceed the value 4.85×10^8 A m^{-1} s^{-1}.

In light of the manner in which the Brezovich criterion was measured, it is clear

that it is at best an upper limit for $H \cdot f$ in the most demanding of application conditions – a whole body system applying a uniform field over an entire thorax of an adult. In practise the conditions are likely to be significantly different – smaller coils, inhomogeneous fields, off-axis field directions – all of which are factors that will reduce eddy current heating. Furthermore, it is clear that the clinical tolerability of a therapeutic administration of hyperthermia to counteract cancer is likely to be much higher than that of a healthy volunteer's experience of discomfort after prolonged periods. As such, the continued use of the Brezovich criterion must be regarded as being of limited value, and as no substitute for the proper measurement of clinical tolerability under therapeutic conditions.

2.4.3 Optimum particle size

The optimum particle size for magnetic hyperthermia is still a matter of debate mainly due to the lack of conclusive data to date comparing the predicted and *in vivo* performance of magnetic nanoparticles for a wide range of tumours. Nevertheless it is physically reasonable to assume that the role of size and size distribution on the heating properties of particles will be both significant and pertinent.

From a biological point of view, particles under 100 nm are considered to be suitable for any application requiring tissue penetration, but more specifically for hyperthermia, the minimum size for coated nanoparticles is approximately within 30 - 40 nm; around 20 nm would be the optimum crystal size for magnetic cores and those around 5 nm are more effective for tumour penetration.[47] From a magnetic point of view, there is a delicate equilibrium to be stuck between the intrinsic properties deriving from the material structure (anisotropy field, saturation magnetisation, etc) and the environmental/experimental conditions employed (for instance, frequency and amplitude of the applied fields).

In order to estimate an optimum particle size, a number of groups have systematically characterised the evolution of hysteresis losses and SAR/ILP values with the particle size in well-known materials – mainly iron and iron oxides – following different theoretical and experimental approaches. Despite the diverse field frequency and amplitude ranges tested so far in these materials, it has not been until now that a convergence of reported results is in sight.

The effects of size distribution in the power dissipation on magnetic fluids was theoretically addressed by Rosensweig in an unprecedented article highlighting the importance of using monodisperse colloids in heating experiments.[44] After a previously published work on the physical limits of magnetic particle hyperthermia,[32] Hergt et al. studied the dependence of SAR on the mean particle size over a broad range of size, finding a very high SAR value (1 kW g^{-1} at 410 kHz and 10 kA m^{-1}, corresponding to an ILP of 24.4 nH m^2 kg^{-1}) for magnetosomes produced by magnetotactic bacteria (30 – 40 nm) in comparison with other iron oxide-based ferrofluids (~10 nm).[48]

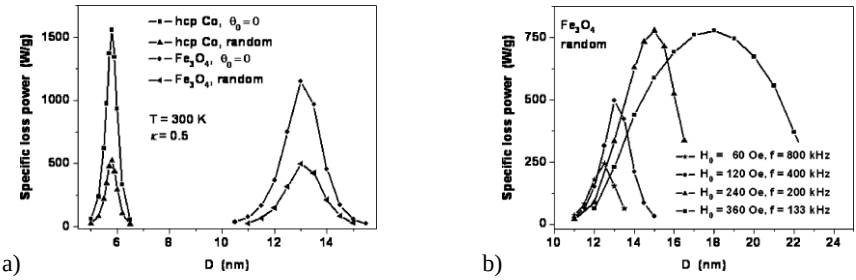

Fig. 5 (a) Specific loss power of oriented and non-oriented assemblies of Co nanoparticles (f = 500 kHz, H = 16 kA m^{-1}) and elongated Fe_3O_4 nanoparticles (f = 400 kHz, H = 9.5 kA m^{-1}) as functions of the particle diameter. (b) SLP of non-oriented assemblies of elongated Fe_3O_4 nanoparticles with aspect ratio b/a = 1.5 as the functions of transverse particle diameter for various frequencies and magnetic field amplitudes when $H \cdot f$ = constant. Reprinted with permission from Ref. [49]. Copyright 2010, American Institute of Physics.

Ma et al.[50] measured the temperature curves of magnetite nanoparticles with average sizes from 7.5 to 416 nm at a frequency of 80 kHz and a field intensity of 32.5 kA m^{-1}. SAR values increase for particle sizes smaller than the exchange length (l_{ex}), which represents the scale of the perturbed area when a spin is unfavourably aligned. The opposite behaviour is observed for particles bigger than l_{ex}.

Simulations of low-frequency hysteresis loops of diluted superparamagnetic nanoparticles with uniaxial anisotropy can provide valuable information about the variation of SAR with particle size.[49] On the one hand, calculated SAR values for oriented 6 nm Co nanoparticles can be as high as 1600 Wg^{-1} at H = 16 kA m^{-1} and f = 500 kHz (ILP = 12.5 nH m^2 kg^{-1}), whereas for the non-oriented case SAR values are three times smaller (Fig. 5a); similar results are obtained for elongated magnetite nanoparticles. On the other hand, SAR curves for a selected set of frequency and amplitude values, for which the product $H \cdot f$ is constant, peak at different particle sizes for magnetite nanoparticles (Fig. 5b). Remarkably, the peaks also widen for increasing H values, suggesting that even samples with a broad size distribution could be suitable for magnetic hyperthermia. This result is consistent with the dependence of the relaxation times on the value of the external magnetic field in the strong nonlinear regime.

Based on the use of the Stoner-Wohlfarth theory for single-domain particles, the Néel-Brown relaxation model, and equilibrium functions, Medahuoi et al. have composed a model that allows for a direct comparison of theoretical simulations and experimental results from hyperthermia experiments carried out in iron nanoparticles with particles sizes ranging from 5.5 to 28 nm.[40] In the low field region, the optimum particle volume (V_{opt}) can be calculated from the Néel-Brown model:

$$V_{opt} = \frac{k_B T}{K} \ln(\pi f \tau_0) \tag{7}$$

where K is the anisotropy constant. For larger fields, the Néel-Brown model is no longer valid and V_{opt} can be worked out from a set of two equations related to the optimum coercivity:[†]

$$\mu_0 H_C = 0.48 \mu_0 H_K \left(1 - \kappa^{0.8}\right) \tag{8}$$

where κ is a dimensionless parameter for the variation of the coercive field that takes into account the field sweeping rate and H_K the anisotropy field, and:[41]

$$\mu_0 H_C = (0.81 \pm 0.04)\,\mu_0 H_{\max} \tag{9}$$

where H_{max} is the maximum field amplitude. In the context of this method, a slightly different approach should be followed in order to perform a quantitative analysis of the experimental data. For this purpose, a coercive field value deduced from magnetic hyperthermia experiments $\mu_0 H_{CHyp}$ is defined as the point of highest slope in $SAR(\mu_0 H_{max})$ functions; additionally, the same effective anisotropy constant K_{eff} is assumed for the studied samples. The evolution of $\mu_0 H_{CHyp}$ with the particle size (Fig. 6a) is then obtained by solving the equation:

$$\mu_0 H_{CHyp} = 0.463\,\mu_0 H_K \left(1 - \left[\frac{k_B T}{K_{eff} V} \ln\left(\frac{k_B T}{4\mu_0 H_{CHyp} M_S V f \tau_0} \right) \right]^{0.8} \right) \tag{10}$$

A good agreement is found between coercivity values obtained from the calculated SARs in Fig. 6b (represented by triangles in Fig. 6a) and the experimental ones (full circles in Fig. 6a).

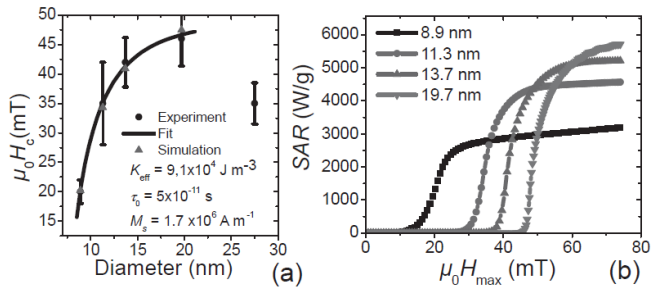

Fig. 6 Quantitative analysis of data at f = 274 kHz. a) Evolution of $\mu_0 H_{CHyp}$ determined from experiments (round dots), from a fit using Equation 10 (solid line), and from the numerical simulations (triangles). M_s = 1.7 × 10^6 A m^{-1}, T = 300 K, f = 274 kHz, τ_0 = 5 × 10^{-11} s and K_{eff} = 9.1 × 10^4 J m^{-3}. b) SAR ($\mu_0 H_{max}$) calculated numerically for four diameters using these parameters. Reprinted with permission from Ref.[40]. Copyright 2010, Wiley.

Given the sometimes intricate relationship among the validity domains for the different magnetisation reversal models available for magnetic particles and their correspondence to the particular magnetic structure, a summary covering all these aspects is provided in Fig. 7.

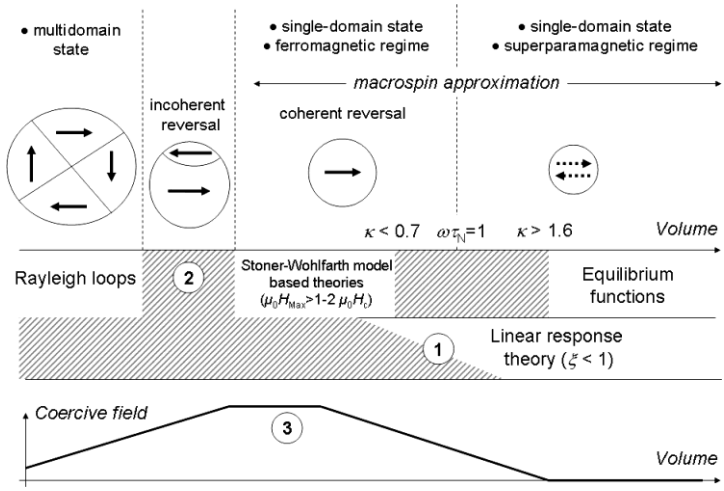

Fig. 7 Schematic representation of the evolution of the magnetic properties of magnetic nanoparticles as a function of their volume and of the models suitable to describe them. The label (1) illustrates that the maximum magnetic field for which the linear response theory (Néel relaxation model) is valid decreases with increasing volume. The label (2) is the domain where incoherent reversal modes occur so Stoner-Wohlfarth model based theories are not valid anymore. The label (3) shows a plateau in the volume dependence of the coercive field. Reprinted with permission from Ref. [41]. Copyright 2011, American Institute of Physics.

2.4.4 Particle shape

Gudoshnikov et al. have studied the hysteresis losses in assemblies of 25 nm magnetite nanoparticles with different shapes and packing densities in the frequency range 10 - 200 kHz at field strengths up to 32 kA m^{-1}, proving that SAR decreases approximately 4.5 times when the sample aspect ratio decreases from 11.4 to 1.[51] Maybe just the qualitative trends found should be considered from these results, since some of the initial approximations made in the model prevent numerical values to be rigorously taken into account.

In addition to its influence in the magnetic properties of an ensemble of particles, shape also affects the way in which nanoparticles are taken up by cells. Spherical gold nanoparticles have been shown to be more easily taken up by HeLa cells than those with a rod-like shape;[52] moreover, rods with an aspect ratio of 1:3 perform better than those with an aspect ratio of 1:5.

2.5 Devices technology for characterisation and clinical practice

Although some commercial devices are available – for example, the *magnetherm* by nanoTherics, the *DM100 series* from nB NanoScale Biomagnetics or the *MFG-1000* from Implementa Hebe AB - most of the systems for experimentation in magnetic particle hyperthermia are purpose-built by research teams. Following are the details of two different solutions.

Resonant Circuits Ltd. (London, UK) has patented a compact and highly configurable device, the MACH (*Magnetic Alternating Current Hyperthermia*) system (Fig. 8). In essence, it embodies three innovations: (i) active feedback to allow precise lock-in and a very high Q-factor, (ii) configuration as a current drive with a very large amplification factor (using 1 A from a power supply the MACH can deliver 100 A to the coil); and (iii) use of a blocking diode to access a negative

voltage swing, and thereby double the accessible field strength from a given supply, and more than treble the accessible frequency of that AC field. Of particular note, it allows for *hand-held* coils to be attached to the heater, and for miniaturisation or even catheterisation of the applicator. Different coil geometries are available depending on the particular application, such as the "pancake" coil for flat surfaces (Fig. 8b) or the "butterfly" coil (Fig. 8a) to ensure a homogeneous field acting over more intricate regions, such as the head or neck.

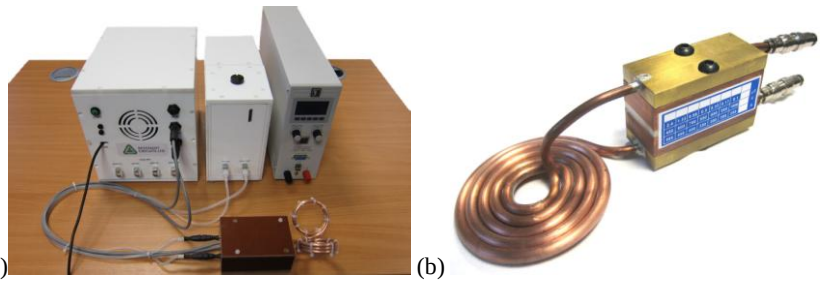

(a) (b)

Fig. 8 (a) Prototype of the Magnetic Alternating Current Hyperthermia (MACH) system with a hand-held butterfly probe. (b) "Pancake" probe option. Courtesy of Resonant Circuits Limited, London, copyright (2011).

MagForce AG (Berlin, Germany) has developed the first alternating magnetic field applicator for humans, the Nanoactivator® (Fig. 9a). This device comprises a resonant circuit at a ferrite yoke that generates a homogeneous 100 kHz alternating magnetic field between two pole shoes above and underneath the treatment aperture.[53] The applicator is complemented with the active ingredient of the therapy, a ferrofluid consisting in a mixture of magnetite and maghemite nanoparticles coated with aminosilanes (NanoTherm®). The aperture clearance can be adjusted in order to ensure a constant field at the treatment site, where the patient lies across. Exposing a tumour previously injected with 3 ml of a 2.1 mol l^{-1} (Fe) magnetic fluid to a magnetic field of 10 kA m^{-1} yields SAR values of 500 W kg^{-1} (ILP = 50 nH m^2 kg^{-1}) in a 10 ml tumour and approximately 100 W kg^{-1} (ILP = 10 nH m^2 kg^{-1}) in a 60 ml tumour volume. In principle, this device can be used for tumours in all parts of the body for lesions up to 5 cm.

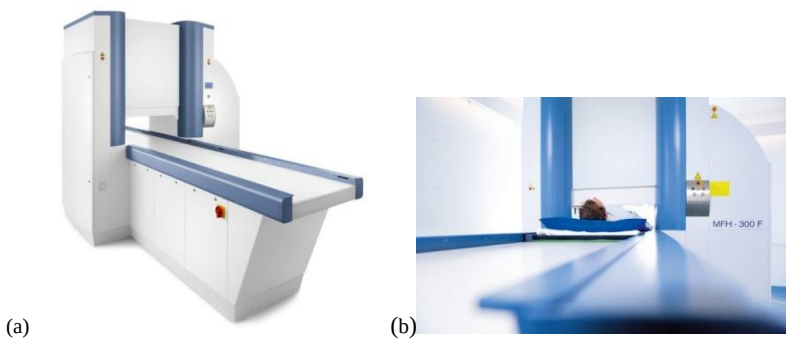

(a) (b)

Fig. 9 (a) General view of the alternating magnetic field applicator for humans NanoActivator™. (b) The patient lies on a slidable coach across the aperture, just at the constant field region. Courtesy of MagForce AG, Berlin, copyright (2011).

3 Biocompatible magnetic colloids for hyperthermia

Many of the new articles published on magnetic hyperthermia are devoted to the synthesis of magnetic nanomaterials with enhanced heating properties and/or targeting capabilities. There is a relatively wide range of materials being currently tested as candidates for magnetic hyperthermia (for example FePt,[54] cobalt ferrites,[55] and NdFeB compounds[56]), but ferrimagnetic iron oxides, maghemite (γ-Fe_2O_3) and magnetite (Fe_3O_4), have become the common choice, for the following reasons:[47]

- Better chemical stability against oxidation than metal nanoparticles
- High magnetisation
- Produce less induced oxidative stress toxicity *in vivo*
- Relatively well known metabolism
- FDA approved for use in humans

Consequently, much of the development made on bespoke nanoparticles for hyperthermia has been built upon the existing knowledge about iron oxide nanoparticles. Moreover, it must be pointed out that many of the available commercial colloids actually are magnetic resonance imaging (MRI) contrast agents. For this reason, the next sections will be dealing with them.

3.1 Chemical synthesis

Two of the most common methods for preparing highly dispersed iron oxide nanoparticles are *thermal decomposition* of iron organometallic compounds and *co-precipitation* of aqueous iron salts (chlorides, nitrates, etc) in basic media. On the one hand, one of the most representative syntheses within the first group is the one reported by Sun et al. to prepare nanoparticles of Fe, Co and Mn ferrites through the decomposition of the corresponding acetylacetonate precursors in benzyl ether in the presence of oleylamine and oleic acid.[57] Since the final aim is to use the nanoparticles in physiological media, solvent exchange and purification techniques are often required for the products of any thermal decomposition method. On the other hand, co-precipitation syntheses result in more suitable water-soluble colloids, and have been widely used in the preparation of maghemite and magnetite nanoparticles.

A close control over pH, reaction time, temperature, precursor and precipitant agent concentration is central to yield the appropriate phase, size and morphology. This has been shown in the case of co-precipitation of Fe^{2+} and Fe^{3+} salts to obtain magnetite nanoparticles using sodium carbonate,[58] which slows down the reaction pathways and hence allows for the tracking of phase transformations. Fig. 10 illustrates the profound changes in phase, morphology and size introduced by increasing reaction pH values. Since most of the magnetic colloids show a size distribution to a certain extent, a size selection process would be needed to further improve the quality of their heating capabilities. If this is not possible during the synthesis stage, it can be later done by magnetic fractionation.[59]

For almost any bioapplication, nanoparticles are usually coated with a range of molecules to ensure their biocompatibility and/or to allow for the coupling of other biomolecules of interest to their surface. Surface coating also retards a quick opsonisation (protein binding) after entering into the bloodstream. These coatings include dextran, polyetyleneglycol, chitosan, aminosilane, glucuronic acid or citric acid, among others, but more and more frequently they include cytotoxic drugs,

antibodies and other markers to target malignant cells more efficiently. This topic will be covered in more detail throughout Sections 3.2 and 3.3.

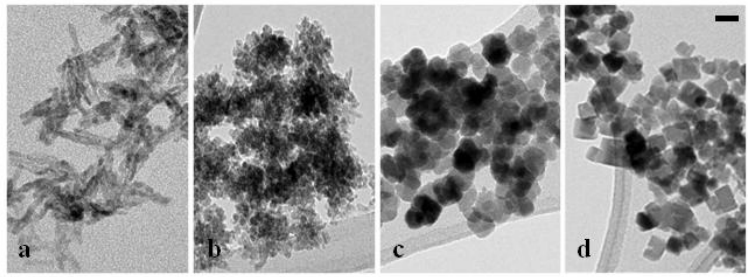

Fig. 10 Iron oxide nanoparticles synthesised by Fe(II)/Fe(III) co-precipitation using sodium bicarbonate as a precipitating agent at pH=7 (a), pH=8 (b), pH=9 (c) and pH=10 (d). The scale bar corresponds to 30 nm. Modified from Ref. [58] with permission from The Royal Society of Chemistry.

3.2 Biodistribution and toxicity

Iron oxide nanoparticles are usually taken up by macrophages in the mononuclear phagocytic system of the liver, spleen, lymphatics, and bone marrow.[60] The associated blood half-lives depend on particle size and coating; smaller nanoparticles have generally longer half-lives and are taken up by lymph nodes, whereas the bigger ones have shorter half-lives and are taken up by the liver and spleen. Particles penetrate the cell in large quantities and are subsequently transferred from early to deep endosomes, remaining in these compartments or, in a very limited extent, degrading due to the fusion of endosomes with lysosomes. Magnetite *in vivo* degradation is believed to induce oxidative stress through the formation of hydroxyl radicals ($HO^{\bullet}$) *via* the Fenton reaction (Eq. 11),[61] which could potentially affect DNA bases; nevertheless, recent *in vitro* studies have discarded any mutagenic effects caused by iron oxide nanoparticles.[62]

$$Fe^{2+} + H_2O_2 \rightarrow Fe^{3+} + HO^{\bullet} + OH^{-} \quad (11)$$

This reaction is intimately related to the Haber-Weiss reaction,[63] where a superoxide radical (O_2^{-}) with hydrogen peroxide to produce an hydroxyl radical:

$$O_2^{-} + H_2O_2 \rightarrow O_2 + HO^{\bullet} + OH^{-} \quad (12)$$

Superoxide radicals are produced in the mitochondrial electron-transport chain as well as by phagocytic and vascular cells.[64] Given the low rate constant of the Haber-Weiss reaction, the *in vivo* generation of hydroxyl radicals is more likely to proceed via reduction of Fe^{3+} ions (Eq. 13) and the resulting Fe^{2+} ones enter the Fenton reaction (Eq. 11).

$$Fe^{3+} + O_2^{-} \rightarrow Fe^{2+} + O_2 \quad (13)$$

Particles under 10 nm are cleared by glomerular filtration, whereas bigger ones undergo removal via the reticular endothelial system.[47] Studies on a murine breast adenocarcinoma cell line (MTG-B) have shown that within the first hour post-injection of bionized nanoferrite (BNF) particles,[65] 95% of the particles are found in either the external plasma membrane or the extracellular space. Regarding the particle uptake by tumoral cells, 50% of the process is completed after two hours and finished after four hours.[66] Anionic maghemite nanoparticles with unbound carboxylate groups at their surface present a non-specific adsorption due to their high affinity for cellular membrane through electrostatic interactions,[67] estimating their efficiency around three orders of magnitude higher than standard dextran-coated iron oxide nanoparticles.

There are a number of factors influencing the toxicity of nanoparticles for use in humans. One of the most relevant is the residence time of nanoparticles inside the body, briefly mentioned before. Both *in vitro* and *in vivo* tests has been carried out in a range of different nanoparticles,[62] but the answer to whether or not a relatively long residence time would be beneficial largely relies on the ability to confine the nanoparticles in the affected region in a controlled way. Hyperthermic treatments are normally administered in a number of sessions, each with a limited exposure time over a more or less extended period depending on the tumour volume, its accessibility or the use of adjunct therapies. Therefore, a longer residence time would be needed in order to keep the concentration of magnetic fluid under a minimum during the overall treatment. In fact, it has been demonstrated that aminosilane-coated iron oxide nanoparticles are still present in the organism one year after injection in the prostate.[29] Degradation also plays an important role in the toxicity of nanoparticles. Recreating intracellular conditions in an *ex vivo* set of experiments Lévy et al. compared the degradation in acidic conditions with a citrate chelating agent of iron oxide nanoparticles coated with citric acid, dextran and aminoalcohol derivatives of glucose, showing that the crystalline structure and magnetic properties remain unchanged upon degradation and subsequent release of iron soluble species.[68] Iron has no carcinogenic properties *per se*, but in apprising the long-debated role of Fenton reaction in oxidative stress processes catalysed by iron species—and not stored in iron proteins such as transferrin or ferritin—we would like to point out the following remarks: (1) the Fenton reaction rate constant is relatively slow (up to ~6×10^3 M^{-1} s^{-1}, although different constants have been reported[63, 69]) and proceeds very slowly for pH values below 3.5—reasonably close to that of the lysosomes;[70] (2) the addition of nitric monoxide ($NO^{\bullet}$) to superoxide radicals is faster than its reduction to Fe^{2+} cations;[64] (3) coating molecules used to prepare iron oxide nanoparticles limit the reactivity of the latter with the environment in comparison to that of uncoated nanoparticles, and finally, (4) any possible risk associated to iron is linked to an overdose, which is considered as a total body iron in excess of 5 g, approximately a hundred times the normal concentration found in males (50-60 mg kg^{-1}). An illustrative example of dose needed in a real clinical application of iron oxide nanoparticles is the magnetic resonance imaging contrast Resovist® (Bayer Schering Pharma AG, Berlin), which is administered in amounts equivalent to about 1% of normal whole-body iron content, as stated in its directions for use.

Although cellular damages associated to iron oxide nanoparticles has been apparently proved to be mild for normal cells,[62] iron overload alone has been lately suggested to have potential therapeutic effects given the altered regulation of iron in

cancerous cells.[71]

3.3 Recent developments

Thomas et al. reported on the synthesis of iron oxide nanoparticles functionalised with three different carboxylic acid ligands: tiopronin (N-(2-mercaptopropionyl)-glycine), oxamic acid and succinic acid (butanedioic acid). Tiopronin-coated particles showed SAR/ILP values sensibly higher than those corresponding to some of the most used commercial solutions, such as Bayer Schering's Resovist® and Micromod's Nanomag® 100 nm nanoparticles (Table 1). The as-synthesised tiopronin-coated nanoparticles were used in *in vitro* tests on *Staphyloccocus aureus* bacteria, showing a total kill of over 10^7 cfu of the bacteria for a concentration of 50 mg/ml. At present, this report seems to be the first one in which magnetic hyperthermia has been used to kill bacteria.

Table 1 Comparison of heating parameters of iron oxide nanoparticles formed in the presence of tiopronin with Resovist and Nanomag 100 nm when placed in an AC magnetic field on a MACH system. Specific absorption rate (SAR) and intrinsic loss power (ILP) are compared for all 3 samples. Adapted from Ref.[72] with permission of The Royal Society of Chemistry.

	SAR (W g^{-1})	ILP (nH m^2 kg^{-1})
Tiopronin-coated	1179	6.1
Resovist®	279	1.5
Nanomag® 100 nm	263	1.4

Another proposed means for maximising the heating capacity of magnetic nanoparticles, and particularly the SAR (see Section 2.4.1), is the combination of a magnetically hard core ($CoFe_2O_4$) and a magnetically soft shell ($MnFe_2O_4$) to produce exchange coupled core-shell particles.[73] SAR values as high as 2,280 W g^{-1} (ILP = 3.28 nH m^2 kg^{-1}) at a frequency of 500 kHz and field amplitude of 37.3 kA m^{-1} have been measured in 15 nm $CoFe_2O_4$@$MnFe_2O_4$ nanoparticles. In view of the reported results so far from different sources, core-shell magnetic nanoparticles tend to show SAR values an order of magnitude higher than those from single-phase nanoparticles. Nevertheless, SAR values out of this trend (2,452 W g^{-1} at 520 kHz and 29 kA m^{-1}, corresponding to an ILP = 5.61nH m^2 kg^{-1}) have been very recently reported for 19 nm iron oxide nanocubes.[74]

One of the approaches for delivering therapeutic agents to tumours is *passive targeting*. This takes advantage of both the high permeability associated to the tumour vasculature and the fluid retention caused by its defective lymphatic system, which leads to particle accumulation over time in the affected tissue. This implies that the concentration of nanoparticles and other macromolecules can be 100 times higher than in normal tissues – albeit that even this is usually not enough to ensure a therapeutic dose at the tumour site.[60]

The other approach is *active targeting*, which makes use of either locally or systemically administered nanoparticles functionalised with antibodies that specifically bind to the targeted tumour, constituting a first step towards tailored treatments. There has been a burgeoning activity around this concept during the past ten years,[14, 75-77] but it has been lately taken to a higher level with the design of *multifunctional nanocarriers*. Cho et al.[78] succeeded in synthesising magnetic nanospheres integrating fluorescent superparamagnetic nanoparticles for multimodal imaging and hyperthermia, specific antibodies for cell targeting and anticancer drugs

for localised treatment (Fig. 11). In this approach, quantum dots with emissions in the near-infrared range are conjugated onto the surface of a nanocomposite consisting of 10 nm magnetite nanoparticles embedded in a 150 nm spherical polystyrene matrix. Subsequently, the chemotherapeutic agent paclitaxel (PTX) is loaded onto their surface by using a layer of biodegradable polylactic-*co*-glycolic acid (PLGA). (Fig. 11a). Ethylendiamine allows for the coupling of anti-prostate specific membrane antigen (anti-PSMA) in order to add targeting capabilities to the system (Fig. 11b,c), resulting in a fully-integrated multifunctional nanocarrier (Fig. 11d). A simple fluorescence imaging test performed in LNCaP prostate cancer cells implanted in mice reveals that these nanocarriers accumulate in tumours, unlike the untreated control samples, where no fluorescence is measured.

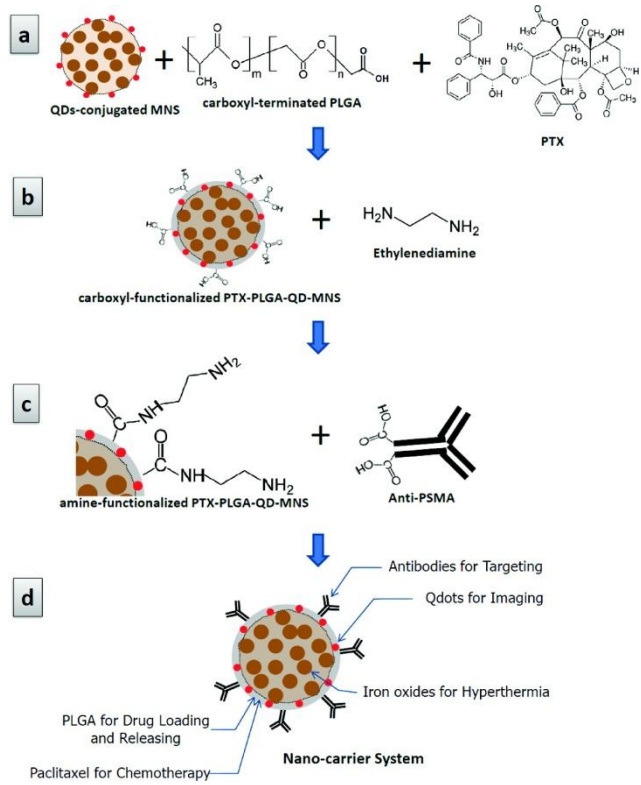

Fig. 11 Schematic diagrams illustrating surface functionalisation of magnetic nanospheres (MNSs): (a) carboxyl functionalisation using carboxyl-terminated PLGA on the surface of QD-MNSs with PTX loading; (b) amine functionalisation by conjugation of ethylenediamine to the surface of carboxylate-functionalised PTX-PLGA-QD-MNSs; (c) conjugation of anti-PSMA to the PTX-PLGA-QD-MNSs, and (d) new multifunctional (fluorescent imaging, targeting, hyperthermia, and chemotherapy) nanocarrier system. Reprinted with permission from Ref. [78]. Copyright (2010) American Chemical Society.

Although not strictly speaking a magnetic hyperthermia application, a notable recent development was put forward by Kim et al. to kill glioblastoma multiforme cancer cells.[79] The idea is to initiate a programmed cell death by mechanically

inducing membrane disruption as a result of the oscillation of magnetic microdiscs under the action of an AC field. The discs are made of a 20:80% iron-nickel alloy with a 5nm gold coating (Fig. 12a), and to specifically target glioma cancer cells, these are biofunctionalised with anti-human-IL13α2R antibody, which is overexpressed on the surface of glioma cells. The magnetic structure of the discs comprises a vortex spin state (Fig. 12b) due to the competition between exchange and magnetic dipole–dipole interactions, and it ideally shows zero magnetisation in the absence of an external field due to the in-plane flux closure. When an alternating magnetic field of 90 Oe and a few tens of Hz is applied, the magnetic discs oscillate (Fig. 12c) inside the cells, exerting a mechanical stress on the membrane and hence compromising its integrity. In comparison with magnetic hyperthermia techniques, this approach offers two remarkable advantages: a much smaller field intensity, approximately 100,000 times smaller, and a reduced treatment time of around ten minutes. That said, the same issues of applying AC fields to remote locations in the body are encountered as in magnetic hyperthermia; and the iron-nickel discs are also likely to show inductive heating at typical hyperthermia frequencies – so that it is conceivable that a combined mechanical/hyperthermic modality might develop from these initial findings.

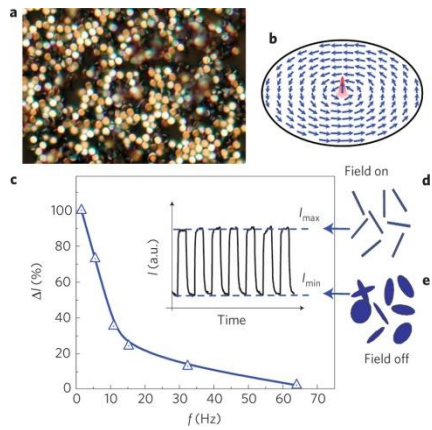

Fig. 12 (a) Reflection optical microscope image of the dried suspension of 60-nm-thick, ~1-μm-diameter 20:80 iron–nickel (permalloy) discs coated with a 5-nm-thick layer of gold on each side. The discs were prepared by means of magnetron sputtering and optical lithography. (b) Micromagnetic model of magnetic-vortex spin distribution. The magnetic vortex consists of a ~10-nm-diameter, perpendicularly magnetised vortex core, and an in-plane flux-closure spin arrangement with zero net magnetisation in the remanent state. (c) Dependence of the light-intensity modulation $\Delta I=I_{max}-I_{min}$ owing to the field-driven disc alignment (e–d) on the applied field frequency f. Inset, A representative time variation of the intensity I of the laser beam travelling through the vial containing the aqueous disc solution subjected to an AC magnetic field. Reprinted by permission from Macmillan Publishers Ltd (Nature Materials): D.H. Kim, E. A. Rozhkova, I. V. Ulasov, S. D. Bader, T. Rajh, M. S. Lesniak and V. Novosad, *Nat Mater*, 2010, 9, 165-171, copyright (2010).

4 Clinical trials: recent case studies

4.1 Bone metastasis

Bone is the most common site of cancer metastasis; moreover, 70% of the patients dying of prostate or breast cancer present evidences of bone metastases, and to a

lesser extent (30 - 40%) bone metastases are also associated with thyroid, kidney and lung cancer. Radiotherapy alone or combined with surgical intervention is the common practice approach to treatment, but is not always a guarantee of success, and can sometimes lead to soft tissue damage.

Matsumine et al..[80] have lately reported the outcome of the first clinical application of hyperthermia in patients of metastatic bone tumours. For this purpose, they have used a cylindrical-coil AC field generator working at a frequency of 1.5 MHz, inside which the affected limb can be inserted for treatment. The clinical strategy consisted of an initial surgical intervention followed by the implantation of a mixture of "bare" magnetite nanoparticles and calcium phosphate cement, which is a biocompatible bone substitute. The procedure was tested on 23 patients presenting 25 metastatic lesions, which were treated with the field generator every two days starting from the eighth day after surgery. The exposure time to the magnetic field was 15 minutes per day. Thirty-two percent of lesions were reduced and presented visible bone formation (Fig. 13), 64% showed no progressive lesions for more than three months and just 4% presented a poor response to the treatment. These results are comparable to those obtained with a combined treatment of radiotherapy and surgical intervention, thus suggesting the effectiveness of hyperthermia in this particular study.

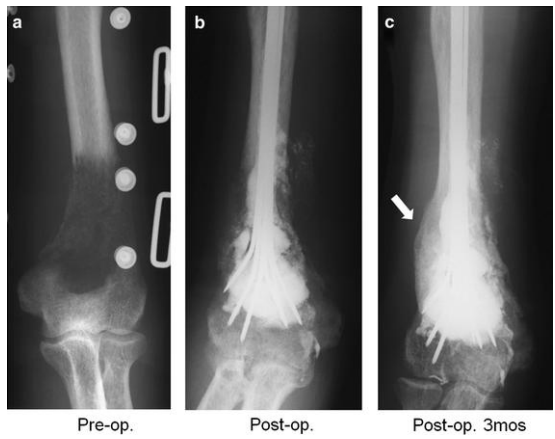

Fig. 13 A radiograph of a bladder cancer that had metastasized to the humerus (a). After curettage of the lesion and reinforcement with wire, CPC containing magnetite was implanted into the cavity (b). At 3 months after undergoing hyperthermia (c), massive new bone formation had become visible (arrow). Reprinted from Ref. [80], with kind permission from Springer Science and Business Media.

4.2 Glioblastoma multiforme

The glioblastoma multiforme (GBM) is the most common and deadly type of brain tumour, with a median life expectancy of twelve months after diagnosis.[81] The data from a recent non-randomised phase II clinical trial by the team of Andreas Jordan have shown improvements in survival times after a combined treatment of magnetic hyperthermia with 12 nm aminosilane-coated magnetite nanoparticles and fractioned stereotactic radiotherapy.[26] After going through both the corresponding feasibility and efficacy studies, this treatment received European regulatory approval in the second half of 2010, covering the treatment of brain tumours throughout the

European Union. The study was conducted on a group of 66 patients of GBM, 59 of which were recurrent cases. On six semi-weekly sessions of one hour each, tumours were treated following the same procedure described elsewhere for the Nanoactivator (see also Section 2.5).[82] Direct temperature measurements through an intracranial thermometry catheter were compared with previously calculated temperatures from the density distribution of the nanoparticles (Fig. 14a-d), their SAR/ILP value and the estimated perfusion at the tumour area.

After analysing all the variables involved that could have an impact on life expectancy, only the tumour volume at the entry point of the study showed a correlation with survival following the first diagnosis of tumour recurrence or progression (OS-2 endpoint of the study). Figures demonstrated an overall increase in survival as reflected from the extension of median OS-2 to 13.4 months compared to 6.2 months in a previous study focused on radiotherapy and chemotherapy in GBM patients. Reported side effects (tachycardia, headaches, overall/local body temperature elevation, etc.) were not severe, indicating that this technique is well tolerated and can be safely applied to recurrent GBM patients. It is worth mentioning that there was no indication of iron being released from the intratumoral deposits or being metabolized.

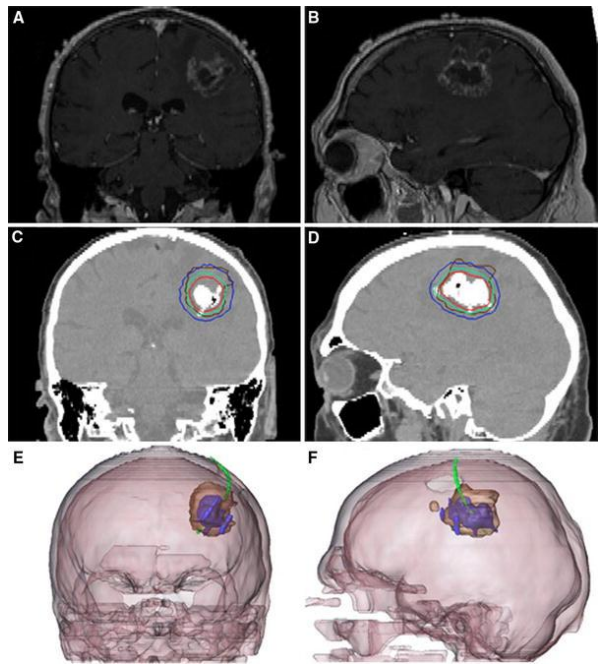

Fig. 14 Glioblastoma recurrence. (a,b) Pre-treatment brain magnetic resonance imaging (MRI). (c,d) Post-instillation computerised tomography (CT) showing magnetic nanoparticle deposits as hyperdense areas. Isothermal lines indicate calculated treatment temperatures between 40°C (*blue*) and 50°C (*red*). The brown line represents the tumour area. (e,f) 3-D reconstruction of fused MRI and CT showing the tumour (*brown*), magnetic fluid (*blue*) and thermometry catheter (*green*). Reprinted from Ref. [26] with kind permission from Springer Science + Business Media.

4.3 Prostate cancer

The heterogeneous and multifocal character observed in many cases of prostate cancer constitutes a real challenge for clinicians and researchers. Early screenings can extend the life expectancy achieved by radical prostatectomy and radiotherapy, but in advanced cases, prostate cancer has metastasised to bone by the time that the disease is detected.[83]

As a continuation of a previous pilot study,[84] Johannsen et al. recently presented the results of two phase I clinical trials focused on the comparison of hyperthermia alone and combined with 125-I permanent seed brachytherapy, i.e. internal radiotherapy. In both trials, magnetite nanoparticles with an aminosilane-like coating and a core size of about 15 nm were instilled in the patients under transrectal ultrasound and fluoroscopy guidance. Hyperthermia sessions were conducted using the Nanoactivator^{TM} field applicator previously described in Section 2.5, operated at a frequency of 100 kHz and field strength between 2.5 – 15 kA m^{-1}. Six thermotherapy sessions were delivered at weekly intervals. Particle localisation were carried out through CT image reconstruction in a similar way to that reported elsewhere.[85] This technique generates a 3D visualisation of the prostate region (Fig. 15) showing the precise location of the nanoparticles. Additionally, a non-invasive temperature calculation can be performed from the iron mass, the applied magnetic field and the SAR of the instilled magnetic fluid. The so-calculated temperature distribution was compared with that obtained through invasive thermometry of the prostate during the first and last sessions.

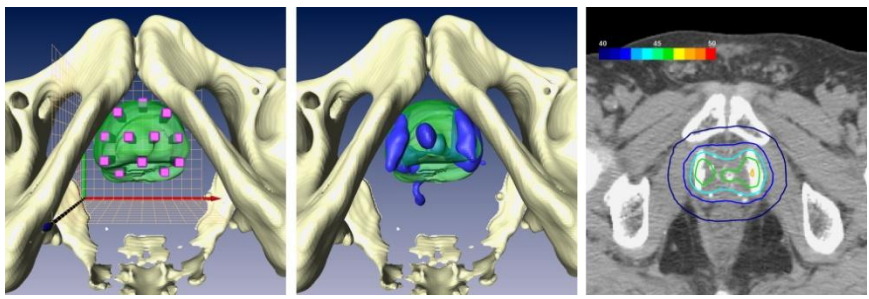

Fig. 15 Three-dimensional reconstructed image of the prostate, viewed from below, illustrating a simplified preplan (left; prostate volume in green, spline probes in red). The three-dimensional image indicates the planned position of the trajectories, where the nanoparticle dispersion is ideally distributed as a continuous deposit moving the needle from the basal to the apical end of the prostate (0.5–1 ml/trajectory). A three-dimensional image of the same patient is shown after the magnetic fluid injection (center; nanoparticle deposits in blue). In the native computed tomography scan of the same patient (right), iron oxide nanoparticle deposits in the prostate appear as regions of higher density compared to the surrounding prostate tissue. Isothermic lines describe calculated intraprostatic temperatures. Reprinted from ref [85] , copyright (2007), with permission from Elsevier.

In the first phase I study, ten patients with recurrent prostate cancer underwent hyperthermia sessions alone, whereas in the second phase I trial eight patients also with recurrent prostate cancer were treated combining hyperthermia and low dose brachytherapy. Intraprostatic median temperatures measured in 90% of the cases (T_{90}) were 40.1 ºC for hyperthermia alone and 39.9 ºC for the combined study. Differences between the planned and actual spatial distribution of the nanoparticles after injection were reported for those patients previously irradiated patients.

Regarding adverse side effects, there is a temporal impairing of patients quality of life and local discomfort has been observed for field intensities over 4-5 kA m^{-1}. The potential efficacy of the proposed therapy was based on the decrease of the serum prostate-specific antigen in both groups of patients.

Given the difficulties in achieving a homogeneous heat distribution due to the different thermal conductivities of the prostate surrounding tissues, these feasibility studies constitute an important step towards the establishment of magnetic particle hyperthermia as a reliable monotherapy for prostate cancer thermal ablation.

Conclusions

The on-going progress of research and development in the field of magnetic hyperthermia, and the ever-widening scope of scientists, engineers and clinicians that it encompasses, has led to significant advances in our understanding. It has also led to the challenging of some long-held positions, such as the belief that intracellular hyperthermia is a more destructive heating mechanism than extracellular heating,[28] or the conviction that a minimum temperature of 43 ºC has to be reached in the target tumour – sometimes referred as the *43 ºC dogma*.[17] At the same time, our increased understanding has highlighted the complexity of the problem, and it is clear that future successes will be dictated by our capacity to develop tailored protocols for a given type of cancer, rather than find a generic multipurpose method.

Another important point requiring well-focused efforts is in reducing the concentration of magnetic fluid to be administered. This may be possible through the incorporation of new materials with better heating properties than iron oxides, the most studied system so far. That said, the 5-10 years time span taken to validate new formulations and go through approval processes to grant their use in humans will delay any advances made down to this route. A faster way to make significant improvements might be to incorporate new elements into the current techniques that have been approved for clinical use, or are soon to be approved. For example, a homogeneous temperature distribution is central for the advancement of hyperthermia as a monotherapy, and even though evident progresses have been made in controlling the temperature distribution in human tissues, matching theoretical calculations with experimental results is, particularly in the case of deep tissues, a challenging but solvable task, that could bring substantial reward.

From a practical point of view, there are already many reports on the synthesis and basic characterisation of iron oxide nanoparticles with potential application in hyperthermia. Theoretical-upper-limit SAR/ILP values have been experimentally reached for some formulations, exceeding those of commercially available materials; therefore, it might be argued that efforts should be now be focused on pushing forward these materials into further tests leading to clinical trials. In addition, clearance mechanisms have to be taken into account in designing new nanoparticles for magnetic hyperthermia. Of particular interest is avoiding quick opsonisation and macrophage phagocytosis to ensure an optimum particle deposition on tumour sites. Another factor linked to the design cycle of new nanomaterials is toxicity. The discrepancies arising from published reports so far indicate that longer-term *in vivo* analyses are needed, along with the implantation of standardised protocols between laboratories, in order to draw sound conclusions on toxicity and clinical acceptability.

Furthermore, it is clear that the research community would benefit from making more efforts to publish comparable data from experimental studies and clinical trials under appropriate conditions. In this regard, the adoption of standardised parameters such as the *cumulative equivalent minutes at 43 ºC* (CEM_{43}), which is the accepted metric for thermal dose assessment, would definitely help. Similarly, with regard to the magnetic heating properties of given particles, the use of the ILP intrinsic loss parameter instead of, or alongside, the SAR specific absorption rate parameter, would also enable better comparisons to be made.

Finally, as well as the challenges ahead, there is also reasons for hope and optimism. Clinical magnetic hyperthermia is already being trialled, and the results so far are certainly encouraging. With diligence and perhaps some luck, we hope that the years to come will see the translation of these current developments into therapies that will bring closer to reality the long-sought changes in quality of life and survival rates for cancer patients.

References

[a] *Dept. of Physics and Astronomy, University College London, Gower Street WC1E 6BT, London, UK. Fax:+44 (0)20 7670 2920; Tel: +44 (0)20 7670 2922; E-mail: d.ponce@ucl.ac.uk*
[b] *Davy-Faraday Research Laboratory, The Royal Institution of Great Britain, 21 Albemarle Street W1S 4BS, London, UK.*
[c] *Institute of Biomedical Engineering, University College London, Gower StreetWC1E 6BT, London, UK. Tel: +44 (0)20 3108 4127; E-mail: q.pankhurst@ucl.ac.uk*

† The appearance of the constant μ_0 in most of the expressions is a natural consequence of the use of the SI unit system, consistent with the Sommerfeld convention $\mathbf{B} = \mu_0 (\mathbf{H} + \mathbf{M})$, where **B** is the magnetic induction, **M** the magnetisation and **H** the magnetic field intensity.

1. C. Eheman, S. J. Henley, R. Ballard-Barbash, E. J. Jacobs, M. J. Schymura, A.-M. Noone, L. Pan, R. N. Anderson, J. E. Fulton, B. A. Kohler, A. Jemal, E. Ward, M. Plescia, L. A. G. Ries and B. K. Edwards, *Cancer*, 2012, **118**, 2338-2366.
2. Cancer Research UK, CancerStats, http://info.cancerresearchuk.org/cancerstats/mortality/all-cancers-combined/, accessed in 2012.
3. National Cancer Institute, State Cancer Profiles, http://statecancerprofiles.cancer.gov/, accessed in 2012.
4. J. Gabriel, *The biology of cancer*, John Wiley & Sons Ltd., Chichester, 2007.
5. J. van der Zee, *Ann. Oncol.*, 2002, **13**, 1173-1184.
6. R. D. Issels, *Eur. J. Cancer*, 2008, **44**, 2546-2554.
7. M. Nikfarjam, V. Muralidharan, C. Malcontenti-Wilson and C. Christophi, *European Journal of Surgical Oncology (EJSO)*, 2003, **29**, 856-861.
8. M. H. Falk and R. D. Issels, *Int. J. Hyperthermia*, 2001, **17**, 1-18.
9. D. Jia and J. Liu, *Expert Rev. Med. Devices*, 2010, **7**, 407-423.
10. R. Hergt and W. Andrä, in *Magnetism in Medicine*, Wiley-VCH Verlag GmbH & Co., 2007, pp. 550-570.
11. G. F. Baronzio and E. D. Hager, *Hyperthermia in cancer treatment: a primer*, Springer Verlag, 2006.
12. B. Thiesen and A. Jordan, *Int. J. Hyperthermia*, 2008, **24**, 467-474.
13. Q. A. Pankhurst, N. T. K. Thanh, S. K. Jones and J. Dobson, *Journal of Physics D-Applied Physics*, 2009, **42**.
14. A. K. Gupta and M. Gupta, *Biomaterials*, 2005, **26**, 3995-4021.
15. P. Moroz, S. K. Jones and B. N. Gray, *Int. J. Hyperthermia*, 2002, **18**, 267-284.

16. Q. A. Pankhurst, J. Connolly, S. Jones and J. Dobson, *J. Phys. D: Appl. Phys.*, 2003, **36**, R167.
17. P. Wust, B. Hildebrandt, G. Sreenivasa, B. Rau, J. Gellermann, H. Riess, R. Felix and P. M. Schlag, *Lancet Oncology*, 2002, **3**, 487-497.
18. A. Jordan and K. Maier-Hauff, *J. Nanosci. Nanotechnol.*, 2007, **7**, 4604-4606.
19. A. Jordan, R. Scholz, P. Wust, H. Fähling and F. Roland, *J. Magn. Magn. Mater.*, 1999, **201**, 413-419.
20. K. M. Krishnan, *IEEE Trans. Magn.*, 2010, **46**, 2523-2558.
21. B. Hildebrandt, P. Wust, O. Ahlers, A. Dieing, G. Sreenivasa, T. Kerner, R. Felix and H. Riess, *Crit. Rev. Oncol./Hematol.*, 2002, **43**, 33-56.
22. C. Roca and L. Primo, in *Hyperthermia in Cancer Treatment: A Primer*, 2006, pp. 92-98.
23. R. K. Gilchrist, R. Medal, W. D. Shorey, R. C. Hanselman, J. C. Parrott and C. B. Taylor, *Ann. Surg.*, 1957, **146**, 596-606.
24. R. Medal, W. Shorey, R. K. Gilchrist, W. Barker and R. Hanselman, *Arch. Surg.*, 1959, **79**, 427-431.
25. R. K. Gilchrist, W. D. Shorey, R. C. Hanselma, F. A. Depeyste, J. Yang and R. Medal, *Ann. Surg.*, 1965, **161**, 890-895.
26. K. Maier-Hauff, F. Ulrich, D. Nestler, H. Niehoff, P. Wust, B. Thiesen, H. Orawa, V. Budach and A. Jordan, *J. Neurooncol.*, 2011, **103**, 317-324.
27. A. Ito, H. Honda and T. Kobayashi, *Cancer Immunol., Immunother.*, 2006, **55**, 320-328.
28. Y. Rabin, *Int. J. Hyperthermia*, 2002, **18**, 194-202.
29. M. Johannsen, B. Thiesen, P. Wust and A. Jordan, *Int. J. Hyperthermia*, 2010, **26**, 790-795.
30. W. Andrä and H. Nowack, in *Magnetism in Medicine. A Handbook*, eds. R. Hergt and W. Andrä, 2007, pp. 550-570.
31. R. Ramprasad, P. Zurcher, M. Petras, M. Miller and P. Renaud, *J. Appl. Phys.*, 2004, **96**, 519-529.
32. R. Hergt, W. Andrae, C. G. d'Ambly, I. Hilger, W. A. Kaiser, U. Richter and H.-G. Schmidt, *IEEE Trans. Magn.*, 1998, **34**, 3745-3754.
33. F. Burrows, C. Parker, R. F. L. Evans, Y. Hancock, O. Hovorka and R. W. Chantrell, *J. Phys. D: Appl. Phys.*, 2010, **43**.
34. C. L. Dennis, A. J. Jackson, J. A. Borchers, P. J. Hoopes, R. Strawbridge, A. R. Foreman, J. van Lierop, C. Gruttner and R. Ivkov, *Nanotechnology*, 2009, **20**.
35. L. Néel, *Annales Geophysicae*, 1949, **5**, 99-136.
36. W. F. Brown, *Physical Review*, 1963, **130**, 1677-1686.
37. M. A. Martsenyuk, Y. L. Raikher and M. I. Shliomis, *Soviet Physics JETP*, 1974, **38**, 413–416.
38. D. Ortega, in *Magnetic nanoparticles: from fabrication to biomedical and clinical applications*, ed. N. T. K. Thanh, CRC Press, 2011.
39. R. Hergt, S. Dutz and M. Zeisberger, *Nanotechnology*, 2010, **21**, 015706.
40. B. Mehdaoui, A. Meffre, J. Carrey, S. Lachaize, L.-M. Lacroix, M. Gougeon, B. Chaudret and M. Respaud, *Adv. Func. Mater.*, 2011, **21**, 4573-4581.
41. J. Carrey, B. Mehdaoui and M. Respaud, *J. Appl. Phys.*, 2011, **109**.
42. P. A. Mason, W. D. Hurt, T. J. Walters, J. A. D'Andrea, P. Gajsek, K. L. Ryan, D. A. Nelson, K. I. Smith and J. M. Ziriax, *IEEE Trans. Microwave Theory Tech.*, 2000, **48**, 2050-2058.
43. M. Kallumadil, M. Tada, T. Nakagawa, M. Abe, P. Southern and Q. A. Pankhurst, *J. Magn. Magn. Mater.*, 2009, **321**, 1509-1513.
44. R. E. Rosensweig, *J. Magn. Magn. Mater.*, 2002, **252**, 370-374.
45. W. J. Atkinson, I. A. Brezovich and D. P. Chakraborty, *IEEE Trans. Biomed. Eng.*, 1984, 70-75.

46. I. A. Brezovich, *Medical Physics Monograph*, 1988, **16**, 82-111.
47. S. E. Barry, *Int. J. Hyperthermia*, 2008, **24**, 451-466.
48. R. Hergt, S. Dutz and M. Roder, *J. Phys.: Condens. Matter*, 2008, **20**, 385214.
49. N. A. Usov, *J. Appl. Phys.*, 2010, **107**, 123909.
50. M. Ma, Y. Wu, H. Zhou, Y. K. Sun, Y. Zhang and N. Gu, *J. Magn. Magn. Mater.*, 2004, **268**, 33-39.
51. S. A. Gudoshnikov, B. Y. Liubimov and N. A. Usov, *AIP Adv.*, 2012, **2**.
52. B. D. Chithrani, A. A. Ghazani and W. C. W. Chan, *Nano Lett.*, 2006, **6**, 662-668.
53. U. Gneveckow, A. Jordan, R. Scholz, V. Bruss, N. Waldofner, J. Ricke, A. Feussner, B. Hildebrandt, B. Rau and P. Wust, *Med. Phys.*, 2004, **31**, 1444-1451.
54. M. S. Seehra, V. Singh, P. Dutta, S. Neeleshwar, Y. Y. Chen, C. L. Chen, S. W. Chou and C. C. Chen, *Journal of Physics D-Applied Physics*, 2010, **43**.
55. E. Pollert and K. Zaveta, in *Magnetic Nanoparticles: From Fabrication to Clinical Applications*, ed. N. T. K. Thanh, CRC Press, Boca Raton, 2012.
56. E. A. Périgo, S. C. Silva, E. M. B. d. Sousa, A. A. Freitas, R. Cohen, L. C. C. M. Nagamine, H. Takiishi and F. J. G. Landgraf, *Nanotechnology*, 2012, **23**, 175704.
57. S. H. Sun, H. Zeng, D. B. Robinson, S. Raoux, P. M. Rice, S. X. Wang and G. X. Li, *JACS*, 2004, **126**, 273-279.
58. C. Blanco-Andujar, D. Ortega, N. K. T. Thanh and Q. A. Pankhurst, *J. Mater. Chem.*, 2012, **22**, 12498.
59. A. Jordan, T. Rheinländer, N. Waldöfner and R. Scholz, *J. Nanoparticle Res.*, 2003, **5**, 597-600.
60. A. Z. Wang, F. X. Gu and O. C. Farokhzad, in *Safety of Nanoparticles: From Manufacturing to medical applications*, ed. T. J. Webster, Springer Verlag, New York, 2008.
61. S. Sharifi, S. Behzadi, S. Laurent, M. L. Forrest, P. Stroeve and M. Mahmoudi, *Chem. Soc. Rev.*, 2012, **41**, 2323-2343.
62. B. Szalay, E. Tátrai, G. Nyírő, T. Vezér and G. Dura, *J. Appl. Toxicol.*, 2012, **32**, 446-453.
63. Z. Radák, *Free radicals in exercise and aging*, Human Kinetics Publishers, 2000.
64. M. J. Burkitt, *Progress in Reaction Kinetics and Mechanism*, 2003, **28**, 75-103.
65. C. Gruttner, K. Muller, J. Teller, F. Westphal, A. Foreman and R. Ivkov, *J. Magn. Magn. Mater.*, 2007, **311**, 181-186.
66. A. J. Giustini, R. Ivkov and P. J. Hoopes, *Nanotechnology*, 2011, **22**.
67. C. Wilhelm, C. Billotey, J. Roger, J. N. Pons, J. C. Bacri and F. Gazeau, *Biomaterials*, 2003, **24**, 1001-1011.
68. M. Lévy, F. Lagarde, V. A. Maraloiu, M. G. Blanchin, F. Gendron, C. Wilhelm and F. Gazeau, *Nanotechnology*, 2010, **21**.
69. M. L. Kremer, *The Journal of Physical Chemistry A*, 2003, **107**, 1734-1741.
70. X. Huang, *Mutation Research - Fundamental and Molecular Mechanisms of Mutagenesis*, 2003, **533**, 153-171.
71. S. P. Foy and V. Labhasetwar, *Biomaterials*, 2011, **32**, 9155-9158.
72. L. A. Thomas, L. Dekker, M. Kallumadil, P. Southern, M. Wilson, S. P. Nair, Q. A. Pankhurst and I. P. Parkin, *J. Mater. Chem.*, 2009, **19**, 6529-6535.
73. J.-H. Lee, J.-t. Jang, J.-s. Choi, S. H. Moon, S.-h. Noh, J.-w. Kim, J.-G. Kim, I.-S. Kim, K. I. Park and J. Cheon, *Nat Nano*, 2011, **6**, 418-422.
74. P. Guardia, R. Di Corato, L. Lartigue, C. Wilhelm, A. Espinosa, M. Garcia-Hernandez, F. Gazeau, L. Manna and T. Pellegrino, *ACS Nano*, 2012, **6**, 3080-3091.
75. M. M. Yallapu, S. F. Othman, E. T. Curtis, B. K. Gupta, M. Jaggi and S. C. Chauhan, *Biomaterials*, 2011, **32**, 1890-1905.

76. E. Katz and I. Willner, *Angewandte Chemie-International Edition*, 2004, **43**, 6042-6108.
77. M. Shinkai, B. Le, H. Honda, K. Yoshikawa, K. Shimizu, S. Saga, T. Wakabayashi, J. Yoshida and T. Kobayashi, *Jpn. J. Cancer Res.*, 2001, **92**, 1138-1145.
78. H.-S. Cho, Z. Dong, G. M. Pauletti, J. Zhang, H. Xu, H. Gu, L. Wang, R. C. Ewing, C. Huth, F. Wang and D. Shi, *ACS Nano*, 2010, **4**, 5398-5404.
79. D.-H. Kim, E. A. Rozhkova, I. V. Ulasov, S. D. Bader, T. Rajh, M. S. Lesniak and V. Novosad, *Nat Mater*, 2010, **9**, 165-171.
80. A. Matsumine, K. Takegami, K. Asanuma, T. Matsubara, T. Nakamura, A. Uchida and A. Sudo, *Int. J. Clin. Oncol.*, 2011, **16**, 101-108.
81. J. Markert, *Glioblastoma Multiforme*, Jones & Bartlett Learning, 2005.
82. F. K. H. van Landeghem, K. Maier-Hauff, A. Jordan, K. T. Hoffmann, U. Gneveckow, R. Scholz, B. Thiesen, W. Bruck and A. von Deimling, *Biomaterials*, 2009, **30**, 52-57.
83. W. J. Catalona, *New Engl. J. Med.*, 1994, **331**, 996-1004.
84. M. Johannsen, U. Gneveckow, L. Eckelt, A. Feussner, N. WaldÖFner, R. Scholz, S. Deger, P. Wust, S. A. Loening and A. Jordan, *Int. J. Hyperthermia*, 2005, **21**, 637-647.
85. M. Johannsen, U. Gneueckow, B. Thiesen, K. Taymoorian, C. H. Cho, N. Waldofner, R. Scholz, A. Jordan, S. A. Loening and P. Wust, *Eur. Urol.*, 2007, **52**, 1653-1662.